THE GEOLOGICAL SOCIETY OF AMERICA®

What sets the size of current ripples?

Mathieu G.A. Lapotre[1], Michael P. Lamb[1], and Brandon McElroy[2]
[1]Division of Geological and Planetary Sciences, California Institute of Technology, Pasadena, California 91125, USA
[2]Department of Geology and Geophysics, University of Wyoming, Laramie, Wyoming 82071-2000, USA

ABSTRACT

Water flowing over sand in fluvial and marine settings often results in the formation of current ripples. Found in modern and ancient deposits on Earth and Mars, ripple stratification records flow directions and fluid properties that are crucial to interpreting sedimentary records. Despite decades of observations of current ripples, there is no universal scaling relation to predict their size or to distinguish them from dunes. Here we use dimensional analysis and a new data compilation to develop a scaling relation that collapses data for equilibrium wavelengths of ripples forming under unidirectional flows. Results show that ripples are larger with more viscous fluids, coarser grains, smaller bed shear stresses, and smaller specific gravity of sediment. The scaling relation also segregates ripples from dunes, highlighting a narrow regime of transitional bedforms that have morphologic properties and sediment transport conditions that overlap with both ripples and dunes. Our analysis shows that previous absolute size–based definitions of ripples and dunes only hold for certain conditions, such as water flows transporting siliciclastic grains on Earth. The new theory allows estimates of ripple sizes in foreign fluids and on other planets, including meter-scale ripples in methane flows on Titan or in viscous brines on Mars.

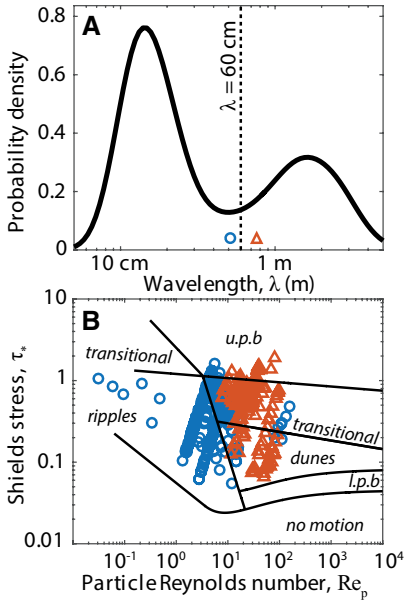

Figure 1. A: Probability density of bedform wavelength (Table DR1; see footnote 1), and the 60 cm threshold of Ashley (1990) (vertical line). B: Bedform stability diagram (from Southard and Boguchwal, 1990a; van den Berg and van Gelder, 2009; as synthesized by Lamb et al., 2012) with ripples (blue circle) and dunes (red triangle) discriminated by the 60 cm threshold. Abbreviations: l.p.b—lower plane bed regime; u.p.b—upper plane bed regime.

INTRODUCTION

Current ripples are migrating waves of sand that form under ocean currents, turbidity currents, and rivers. They tend to be 10–20 cm in wavelength (λ), but can be found in sizes ranging from ~8 cm to as large as ~60 cm (e.g., Middleton and Southard, 1984) (Fig. 1A). Current ripples arise from a spatial lag between shear stresses exerted by the flow on the bed and sediment flux (Smith, 1970; Richards, 1980; Charru et al., 2013), and linear stability analysis shows that their initial wavelength either scales with the thickness of the viscous sublayer or a sediment-transport saturation length, $L_{sat} \propto \frac{u_* D}{\sqrt{RgD}}$ (where u_* is bed shear velocity, D is grain diameter, $R = \frac{\rho_s - \rho_f}{\rho_f}$ is submerged specific density of sediment with ρ_s and ρ_f the sediment and fluid densities, respectively, and g is gravitational acceleration; Charru et al., 2013). Once initiated, ripples grow until they reach an equilibrium wavelength (Betat et al., 2002); however, there exists no universal theory to predict it. Ripples are generally considered distinct from dunes in that (1) they are typically smaller ($\lambda < 60$ cm) (Ashley, 1990) (Fig. 1A), (2) they compose the smaller mode of what is often a bimodal distribution of sandy bedforms under unidirectional flows (Middleton and Southard, 1984) (Fig. 1A), and (3) distinct physical processes are thought to control their formation and size (e.g., Bennett and Best, 1996). For example, dunes are thought to increase in size with increasing flow depth and flow velocity and finer grain size (Southard and Boguchwal, 1990a), behaviors that are not typically observed for ripples. Ripple size, in contrast, is typically thought to be insensitive to flow velocity (Baas, 1994) and to increase with grain size (Allen, 1982; Raudkivi, 1997). However, a dynamical difference between ripples and dunes is debated. For example, Jerolmack and Mohrig (2005) proposed that ripples and dunes are similar on the basis of spectral analysis of a riverbed that showed that all scales of sandy bedforms coexist, spanning ripples and dunes. Thus, the bimodality of bedform wavelengths in Figure 1A might result from experimental or observational bias. Furthermore, Bartholdy et al. (2015) proposed that ripple size should scale with flow depth, an attribute normally associated with dunes. It is also unclear if the 60 cm break in scale proposed by Ashley (1990) (Fig. 1A) provides a universal discriminant of ripples and dunes that can be applied on different planets, or whether it results from the similarity of sediment and fluid properties found on Earth (Lamb et al., 2012). These studies highlight the need to unify previous work and develop a dynamic scaling relation for the equilibrium size of ripples that encompasses grain size, flow strength, sediment and fluid properties, and gravity.

Multiple studies have compared the size of ripples to various bed and flow characteristics. Yalin (1985) proposed that bedform wavelength depends on a number of flow and sediment parameters, but found that the wavelength of smaller bedforms (ripples) is proportional to the thickness of the viscous sublayer, i.e., $\lambda \propto \nu/u_*$ (where ν is kinematic viscosity of the fluid). In contrast, other studies suggested that ripple size scales with $\nu^{2/3}$ (e.g., Boguchwal and Southard, 1990; Lamb et al., 2012), but does not vary with u_* (e.g., Baas, 1994). In addition to fluid properties, bed characteristics also affect ripple size. Ripple wavelength has been proposed to increase with grain size following linear (Allen, 1982), power-law (Raudkivi, 1997), and logarithmic (Baas, 1999) relations. Middleton and Southard (1984) suggested that wavelength appears to decrease with increasing grain density, a finding that is also supported by dimensional analysis (Boguchwal and Southard, 1990). However, a single relation has yet to be proposed that can reproduce all observed ripple size dependencies across wide ranges in grain size, viscosity, density, and flow strength.

Ripple theory provides a powerful proxy to decipher past and present environmental conditions on Earth and other planetary bodies, and

Data Repository item 2017063 | doi:10.1130/G38598.1

has been used to infer the existence of water flows, viscous brines, and a low-density paleoatmosphere on Mars (Southard and Boguchwal, 1990b; Lamb et al., 2012; Lapotre et al., 2016). Current ripples also are hypothesized to exist in rivers of methane on Titan (Burr et al., 2013; Grotzinger et al., 2013). However, proper interpretation of ripples on other planets requires a dimensionless scaling relation that accounts for material properties and gravity that differ from those of Earth. Given that the Shields stress (τ_*) and particle Reynolds number (Re_p) reasonably segregate the occurrence of ripples and dunes (e.g., Lamb et al., 2012) (Fig. 1B), it seems reasonable that these dimensionless quantities also affect ripple size.

Based on dimensional analysis and a comprehensive data compilation, we propose herein a new dimensionless number, the Yalin number, that allows for a unifying scaling relation for equilibrium ripple size. This work builds on that in Lapotre et al. (2016), where a similar dimensionless scaling relation for analysis of large wind ripples on Mars was proposed, but an exhaustive data compilation of current ripples and dunes was not analyzed. Herein we show that ripple size data collapse into a dimensionless relation with the Yalin number, which also yields a process-based discriminant of the ripple-dune transition that is applicable for wide ranges in fluids and sediment properties and gravity.

THEORY

Physical parameters often attributed to bedform stability are fluid kinematic viscosity, ν (m^2/s), total bed shear velocity (skin friction + form drag), u_* (m/s), grain diameter, D (m), and submerged specific gravity of sediment, Rg (m/s^2) (e.g., Boguchwal and Southard, 1990). These four quantities can be recast in terms of two dimensionless parameters. While the choice of these parameters is nonunique, here we choose the particle Reynolds number, $Re_p = \frac{u_* D}{\nu}$, and Shields stress, $\tau_* = \frac{u_*^2}{RgD}$ (Fig. 1B). Others have used different but mathematically equivalent combinations of these parameters (Boguchwal and Southard, 1990; van den Berg and van Gelder, 1993). Current-ripple wavelength, which has been argued to scale with the thickness of the viscous sublayer (Yalin, 1985), or ν/u_*, introduces another variable. Following the same dimensional analysis, a third dimensionless variable becomes the dimensionless wavelength, $\lambda^* = \frac{\lambda u_*}{\nu}$.

Yalin (1985) argued that the number of dimensionless parameters controlling ripple size can be further reduced to two by showing that ripple-wavelength data collapsed into the (X_y, Y_y) parameter space, where $X_y = 3.38 Re_p^{1/2} \tau_*^{1/4}$, and $Y_y = \frac{\lambda}{3.38D} \frac{Re_p^{1/2}}{\tau_*^{1/4}}$. We recast the latter parameters to isolate λ^* as

$$\begin{cases} \chi = \dfrac{X_y^2}{11.42} = Re_p \sqrt{\tau_*} \\ \lambda^* = X_y Y_y = \dfrac{\lambda u_*}{\nu} \end{cases} . \quad (1)$$

We name the new parameter χ the Yalin number, after Mehmet Selim Yalin. The Yalin number can be interpreted as a metric for the susceptibility of a grain on the bed to be entrained by fluid flow, which not only depends on flow strength relative to the particle weight (τ_*), but also on the degree to which the particle is immersed within the viscous sublayer (Re_p) (e.g., Niño et al., 2003). The Yalin number also is proportional to $\frac{L_{sat} u_*}{\nu}$, a metric previously proposed to control initial ripple wavelength (Charru et al., 2013). To explore this new parameter space, we compiled wavelength data for both ripples and dunes inferred to be at steady-state morphology; these data cover a wide range of fluid and sediment properties, including high-viscosity fluids (e.g., Grazer, 1982), and thus a wide range in χ (Table DR1 in the GSA Data Repository[1]). Our new compilation comprises 472 data points, from 15 flume and field studies, each of which is an average of tens of bedform-size measurements (Table DR1).

RESULTS

We first consider the often-used criterion of Ashley (1990) that classifies <60-cm-wavelength bedforms as ripples (Fig. 1). Figure 1B shows that while this criterion is overall consistent with commonly used bedform stability diagrams, a few bedforms that would be interpreted as ripples from a size-threshold criterion would be classified as dunes using the criteria of Southard and Boguchwal (1990a) and van den Berg and van Gelder (1993), based on morphology. The inconsistency between the absolute size definition of Ashley (1990) and the bedform stability diagrams highlights the need for a better discriminant between ripples and dunes.

Figure 2A shows our data compilation in (χ, λ^*) space. Most of the smaller bedforms collapse to a single power-law relation ($R^2 = 0.79$),

$$\lambda^* = 2504 \chi^{1/3}. \quad (2)$$

Based on this dimensional analysis, we expect such a collapse for ripples in this parameter space, whereas dunes are not expected to collapse because this space does not account for parameters such as flow depth, which is known to partially control dune size (e.g., Southard and Boguchwal, 1990a). We thus interpret those bedforms that collapse to Equation 2 as ripples, which also correspond to $\chi < \sim 4$. For $4 \le \chi \le 9$, there is a sharp, order of magnitude, increase in λ^*. The larger bedforms, at $\chi > \sim 9$, do not collapse to a single relation in this parameter space, and we therefore interpret them as dunes.

[1]GSA Data Repository item 2017063, supplementary figures and table, is available online at www.geosociety.org/datarepository/2017, or on request from editing@geosociety.org.

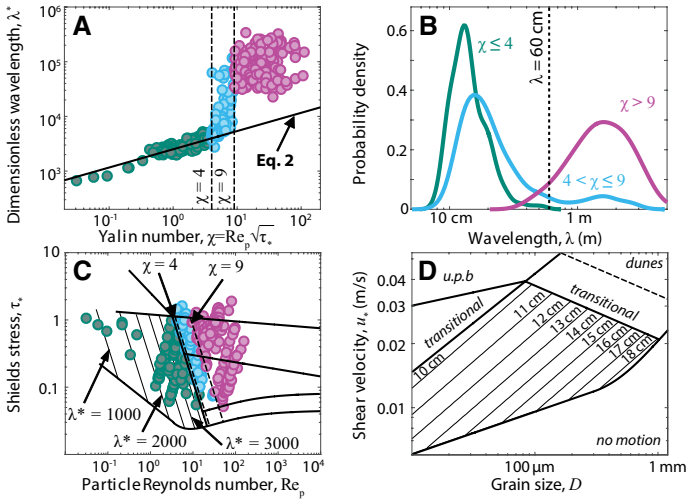

Figure 2. A: Dimensionless bedform wavelength versus Yalin number (see text). Bedforms are discriminated by thresholds in χ (ripples in green, transitional in blue, dunes in pink). Best fit to ripple data, $\lambda^* = 2445\chi^{0.38}$ ($R^2 = 0.80$), is statistically indistinguishable from Equation 2. B: Probability density of bedform wavelength discriminated by Yalin numbers. C: Bedforms classified by Yalin number on bedform stability diagram from B. Bedform regimes are as in Figure 1B. Contours in the ripple regime indicate lines of constant λ^* at intervals of 500. D: Close-up of the ripple field in dimensional bedform stability diagram with predicted ripple wavelength for freshwater on Earth (R = 1.65, g = 9.81 m/s², $\nu = 10^{-6}$ m²/s) (u.p.b—upper plane bed regime).

Our new definition of ripples and dunes, based on Yalin number, is consistent with the 60 cm threshold of Ashley (1990) for the majority of the data. Figure 2B shows that bedforms with $\chi < 4$ have wavelengths generally <60 cm, with a mode at 12 cm, consistent with sizes commonly attributed to ripples. In contrast, bedforms with $\chi > 9$ are generally >60 cm, and therefore consistent with previous definitions of dunes based on size. Bedforms with $4 \le \chi \le 9$ have wavelengths from both size modes (Fig. 2B) and are skewed to somewhat larger wavelengths than ripples (Fig. 2B). It is also consistent that the boundary between ripples and dunes in the bedform stability diagram (Fig. 2C) appears to be a line of constant χ (i.e., $\mathrm{Re}_p \propto \tau_*^{-1/2}$ or $L_{sat} \propto \nu/u_*$), with $\chi = 4$ matching well the ripple regime upper bound (Fig. 2C). Thus, the Yalin number discriminates between small sandy bedform data that collapse to a single relation in (χ, λ^*) space and data from larger bedforms that do not collapse, providing a process-based, rather than absolute size–based, metric to distinguish between ripples and dunes.

The collapse of ripple data allows for ripple size to be predicted as a function of sediment and fluid properties, such that λ^* can be contoured in bedform stability space (Fig. 2C). In particular, Equation 2 can be rearranged in dimensional form as

$$\lambda = 2504 \frac{\nu^{2/3} D^{1/6}}{(Rg)^{1/6} u_*^{1/3}}, \quad (3)$$

which is valid within the ripple stability field (Fig. 2D), and unifies previously proposed scaling relations that focused on single dependencies of ripple size. For example, the dependence on kinematic viscosity to the 2/3 power (Fig. 3A) was inferred from dimensional analysis in multiple studies (e.g., Middleton and Southard, 1984). Yalin (1985) argued that ripple wavelength scales linearly with kinematic viscosity (i.e., λ^* is constant); however, his data set did not cover as wide of a range in χ as in our Figure 2A, and thus the relation $\lambda^* \propto \chi^{1/3}$ was not evident. Equation 3 is consistent with previously published grain-size dependencies (Raudkivi, 1997; Baas, 1999), and shows an increase of ripple wavelength with grain size (Fig. 3B). Earlier studies suggested that there is no dependence of ripple wavelength on flow strength (e.g., Baas, 1994), that $\lambda \propto u_*^{-1}$ (Yalin, 1985), or that wavelength increases with flow strength (e.g., Baas, 1999). We find a weak decreasing trend of wavelength with shear velocity for ripples ($\chi < 4$; Fig. 3C), and the bedforms analyzed by Baas (1999) are in the transitional regime ($4 \le \chi \le 9$) by our definition. Equation 3 is also consistent with predictions from Southard and Boguchwal (1990b) showing a decrease in ripple wavelength with increasing specific submerged density (Fig. 3D). Although Bartholdy et al. (2015) suggested that ripple wavelength depends on flow depth, we observed no improvement in the collapse of ripple data ($\chi < 4$) by further regressing based on flow depth; many of the data they used for comparison are in our transitional ($4 \le \chi \le 9$) or dune ($\chi > 9$) regimes.

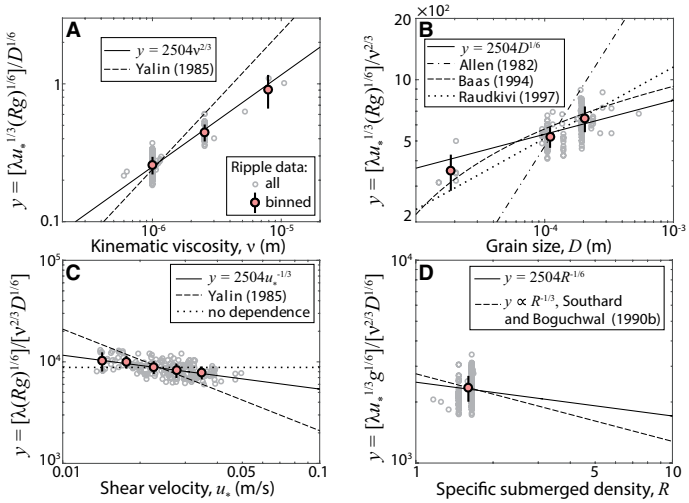

Figure 3. Dependence of normalized ripple wavelength on kinematic viscosity (A), grain size (B), shear stress (C), submerged specific density (D) as compared to Equation 3. See text for variables. Red-filled symbols are binned data, and error bars represent the geometric standard deviation within each bin. Normalized ripple wavelength (*y* axes) was computed by rearranging Equation 3 to isolate the parameter of interest (*x* axes) and eliminating constants. Solid line in each plot represents Equation 3.

DISCUSSION AND CONCLUSION

The collapse of ripple data to Equation 2, and the failure of dune data to collapse in the same parameter space, supports the hypothesis that different physical processes are involved in the formation of ripples and dunes. Importantly, the χ threshold for the upper bound on the ripple regime is more consistent with bedform stability diagrams (Fig. 1A) than the absolute size threshold of Ashley (1990) (Fig. 2C). Our analysis highlights a transition zone across the ripple-dune boundary ($4 \le \chi \le 9$). Transitional bedforms tend to have wavelengths <60 cm, typical of ripples, and yet plot in the dune regime based on previous bedform stability diagrams, where sediment transport is more vigorous (Fig. 1B). Transitional bedforms thus may be a hybrid between ripples and dunes, for which dominant physical processes responsible for both ripples and dunes are operative. The Yalin number separates bedform data into two distinct wavelength modes, but the absolute size break of 60 cm likely results from an observational bias reflecting little variation in sediment and fluid properties, and gravity, investigated in most studies. For example, at the upper bound of the ripple regime $\chi \approx 4$ and $\lambda^* \approx 4000$, which when combined yields $\lambda \approx 2000 \nu^{1/2} \left(\frac{D}{Rg}\right)^{1/4}$. Thus, the χ threshold implies a different absolute size break between ripples and dunes for different viscosity and density fluids, different sediment sizes and densities, and different gravitational acceleration.

Why does the ripple domain exist for Yalin numbers less than four? Previous workers suggested that ripples form under hydraulically smooth flow (defined as a roughness Reynolds number <5; Nikuradse, 1933), or when the laminar sublayer is thicker than a grain diameter ($\mathrm{Re}_p < \sim 11.6$; Engelund and Hansen, 1967), both of which are vertical lines in Figure 2C that are not consistent with the observed sloping ripple-dune boundary. Another hypothesis is that ripples predominantly form under bedload transport (e.g., Richards, 1980); however, the suspension threshold of Niño et al. (2003) also differs from a constant χ (Fig. DR1). While a constant χ implies that L_{sat} is a multiple of viscous sublayer thickness, it is unclear why such a criterion would control the ripple-dune transition. Bennett and Best (1996) attributed the ripple-dune transition to turbulent wake instabilities shed by ripples, leading to the formation of abnormally large ripples (Leeder, 1983) or bedform mergers that grow dunes (Fernandez et al., 2006). Ultimately, changes in the separation wake may be tied to a certain value of λ^* because it is a ripple-scale Reynolds number. For example, $\lambda^* \approx 4000$ approximately matches the onset of fully developed turbulence downstream of backward-facing steps (e.g., Armaly et al., 1983).

Equation 3 shows that if ν, g, and R do not vary significantly, as is often the case on Earth, then ripple size is a function of D and u_* only. If grain size and wavelength can be estimated from field observations, then Equation 3 can be used to calculate formative bed shear velocity, which can be related to current velocity. Figure 2D, for example, shows predicted ripple wavelengths that range from 8 to 18 cm for decreasing shear velocities, assuming fluid and sediment properties typical for Earth ($g = 9.81$ m/s^2, $R = 1.65$, $\nu = 10^{-6}$ m^2/s). Ripple size is more sensitive to kinematic viscosity than it is to bed shear velocity, and thus might be a better indicator of current or ocean paleotemperatures. For freshwater, a 10 °C change in temperature has an equivalent effect on ripple wavelength, through kinematic viscosity, as a twofold change in bed shear velocity.

Preserved ripple strata in martian sandstones were observed and proposed to have formed in highly concentrated brines (Lamb et al., 2012). Fluvial transport on Titan may also form ripples when ice grains are transported by methane flows (Burr et al., 2013). Because gravity, density, and viscosity are implicitly taken into account, Equation 2 can be applied to other planetary bodies. For example, equivalent freshwater flows on Mars would make ripples 14% larger than on Earth (e.g., for R = 1.65 and g = 9.81 m/s^2 on Earth, and R = 1.9 and g = 3.78 m/s^2 on Mars), consistent with Southard and Boguchwal (1990b). A different kinematic viscosity, such as for viscous brines on Mars (e.g., $\nu = 4 \times 10^{-5}$ m^2/s, R = 1.04) or methane flows on Titan (e.g., $\nu = 5 \times 10^{-6}$ m^2/s, R = 0.85, g = 1.35 m/s^2), has a more significant effect on ripple size. For D = 400 µm and $u_* = 0.02$ m/s, predicted wavelengths are of ~0.15, 2.3, and 0.7 m in freshwater on Earth, brines on Mars, and ice grains in methane flows on Titan, respectively (Fig. DR2). Large ripples in viscous brines may be so large that they are limited in height by flow depth, as inferred in Lamb et al. (2012), further complicating traditional definitions of ripples and dunes.

In summary, data for small sandy bedforms collapse to a single relation in dimensionless wavelength and Yalin number space. This observation and the lack of collapse for larger bedforms imply that different physical processes are involved in the formation of ripples and dunes. The new scaling relation allows for improved paleohydraulic reconstructions based on current ripple size on Earth and other planetary bodies with different gravitational acceleration and exotic sediments and fluids.

ACKNOWLEDGMENTS

We thank J. Southard, W. Fischer, and R. Ewing for discussions that motivated this work, and three anonymous reviewers and M. Perillo for comments that improved our manuscript.

REFERENCES CITED

Allen, J.R.L., 1982, Sedimentary structures, their character and physical basis: Developments in Sedimentology Volume 30: New York, Elsevier, 593 p.

Armaly, B.F., Durst, F., Pereira, J., and Schonung, B., 1983, Experimental and theoretical investigation of backward-facing step flow: Journal of Fluid Mechanics, v. 127, p. 473–496, doi:10.1017/S0022112083002839.

Ashley, G.M., 1990, Classification of large-scale subaqueous bedforms: A new look at an old problem: Journal of Sedimentary Research, v. 60, p. 160–172, doi:10.2110/jsr.60.160.

Baas, J.H., 1994, A flume study on the development and equilibrium morphology of current ripples in very fine sand: Sedimentology, v. 41, p. 185–209, doi:10.1111/j.1365-3091.1994.tb01400.x.

Baas, J.H., 1999, An empirical model for the development and equilibrium morphology of current ripples in fine sand: Sedimentology, v. 46, p. 123–138, doi:10.1046/j.1365-3091.1999.00206.x.

Bartholdy, J., Ernstsen, V.B., Flemming, B.W., Winter, C., Bartholoma, A., and Kroon, A., 2015, On the formation of current ripples: Scientific Reports, v. 5, p. 1–9, doi:10.1038/srep11390.

Bennett, S., and Best, J., 1996, Mean flow and turbulence structure over fixed ripples and the ripple-dune transition, *in* Ashworth, P.J., et al., eds., Coherent flow structures in open channels: Hoboken, New Jersey, John Wiley, p. 67–125.

Betat, A., Kruelle, C.A., Frette, V., and Rehberg, I., 2002, Long-time behavior of sand ripples induced by water shear flow: European Physical Journal E, v. 8, p. 465–476, doi:10.1140/epje/i2001-10110-y.

Boguchwal, L.A., and Southard, J.B., 1990, Bed configurations in steady unidirectional water flows. Part 1. Scale model study using fine sands: Journal of Sedimentary Research, v. 60, p. 649–657, doi:10.1306/212F923C-2B24-11D7-8648000102C1865D.

Burr, D.M., Perron, J.T., Lamb, M.P., Irwin, R.P., Collins, G.C., Howard, A.D., Sklar, L.S., Moore, J.M., Adamkovics, M., and Baker, V.R., 2013, Fluvial features on Titan: Insights from morphology and modeling: Geological Society of America Bulletin, v. 125, p. 299–321, doi:10.1130/B30612.1.

Charru, F., Andreotti, B., and Claudin, P., 2013, Sand ripples and dunes: Annual Review of Fluid Mechanics, v. 45, p. 469–493, doi:10.1146/annurev-fluid-011212-140806.

Engelund, F., and Hansen, E., 1967, A monograph on sediment transport in alluvial streams: Copenhagen, Denmark, Teknisk Forlag Skelbrekgade 4, 63 p.

Fernandez, R., Best, J., and Lopez, F., 2006, Mean flow, turbulence structure, and bed form superimposition across the ripple-dune transition: Water Resources Research, v. 42, W05406, doi:10.1029/2005WR004330.

Grazer, R.A., 1982, Experimental study of current ripples using medium silt [M.S. thesis]: Cambridge, Massachusetts Institute of Technology, 131 p.

Grotzinger, J.P., Hayes, A.G., Lamb, M.P., and McLennan, S.M., 2013, Sedimentary processes on Earth, Mars, Titan, and Venus: Comparative Climatology of Terrestrial Planets, v. 1, p. 439–472.

Jerolmack, D.J., and Mohrig, D., 2005, A unified model for subaqueous bed form dynamics: Water Resources Research, v. 41, W12421, doi:10.1029/2005WR004329.

Lamb, M.P., Grotzinger, J.P., Southard, J.B., and Tosca, N.J., 2012, Were aqueous ripples on Mars formed by flowing brines?, *in* Grotzinger, J.P., and Milliken, R.E., eds., Sedimentary geology of Mars: SEPM (Society for Sedimentary Geology) Special Publication 102, p. 139–150, doi:10.2110/pec.12.102.0139.

Lapotre, M.G.A., et al., 2016, Large wind ripples on Mars: A record of atmospheric evolution: Science, v. 353, p. 55–58, doi:10.1126/science.aaf3206.

Leeder, M., 1983, On the interactions between turbulent flow, sediment transport and bedform mechanics in channelized flows, *in* Collinson, J.D., and Lewin, J., eds., Modern and ancient fluvial systems: International Association of Sedimentologists Special Publication 6, p. 5–18, doi:10.1002/9781444303773.ch1.

Middleton, G.V., and Southard, J.B., 1984, Mechanics of sediment movement (second edition): Society of Economic Paleontologists and Mineralogists Short Course 3, 401 p.

Nikuradse, J., 1933, Stromungsgesetz in rauhren rohren: Verein Deutscher Ingenieure Forschungshefte 361, 22 p. [Laws of flow in rough pipes, 1950: Washington, D.C., National Advisory Commission for Aeronautics Technical Memorandum 1292, 64 p.

Niño, Y., Lopez, F., and Garcia, M., 2003, Threshold for particle entrainment into suspension: Sedimentology, v. 50, p. 247–263, doi:10.1046/j.1365-3091.2003.00551.x.

Raudkivi, A.J., 1997, Ripples on stream bed: Journal of Hydraulic Engineering, v. 123, p. 58–64, doi:10.1061/(ASCE)0733-9429(1997)123:1(58).

Richards, K.J., 1980, The formation of ripples and dunes on an erodible bed: Journal of Fluid Mechanics, v. 99, p. 597–618, doi:10.1017/S002211208000078X.

Smith, J.D., 1970, Stability of a sand bed subjected to a shear flow of low Froude number: Journal of Geophysical Research, v. 75, p. 5928–5940, doi:10.1029/JC075i030p05928.

Southard, J.B., and Boguchwal, L.A., 1990a, Bed configurations in steady unidirectional water flows. Part 2. Synthesis of flume data: Journal of Sedimentary Research, v. 60, p. 658–679, doi:10.1306/212F9241-2B24-11D7-8648000102C1865D.

Southard, J.B., and Boguchwal, L.A., 1990b, Bed configurations in steady unidirectional water flows. Part 3. Effects of temperature and gravity: Journal of Sedimentary Research, v. 60, p. 680–686, doi:10.2110/jsr.60.680.

van den Berg, J.-I., and van Gelder, A., 1993, A new bedform stability diagram, with emphasis on the transition of ripples to plane bed in flows over fine sand and silt, *in* Marzo, M., and Puigdefábregas, C., eds., Alluvial sedimentation: International Association of Sedimentologists Special Publication 17, p. 11–21, doi:10.1002/9781444303995.ch2.

Yalin, M.S., 1985, On the determination of ripple geometry: Journal of Hydraulic Engineering, v. 111, p. 1148–1155, doi:10.1061/(ASCE)0733-9429(1985)111:8(1148).

Manuscript received 13 September 2016
Revised manuscript received 24 November 2016
Manuscript accepted 28 November 2016

Printed in USA